The Muscarinic Receptor of Chick Embryo Cells: Correlation between Ligand Binding and Calcium Mobilization

GÜNTER OETTLING, HEINRICH SCHMIDT, and ULRICH DREWS
Institute of Anatomy, University of Tübingen, D-7400 Tübingen, Federal Republic of Germany

ABSTRACT In this report we characterize muscarinic cholinergic receptor on embryonic cells. We established dose-response curves by fluorometric measurement of Ca^{2+} mobilization in cell suspensions of whole chick embryos stage 23/24. Ca^{2+} mobilization was quantitated by standardization of chlorotetracycline (CTC) fluorescence changes after stimulation with muscarinic agonists. We determined ED_{50} values for the agonists acetylcholine and carbachol as 3.4×10^{-6} and 2.7×10^{-5} M, respectively. Pilocarpine and oxotremorine were found to act as reversible competitive antagonists with inhibition constants (K_I) of 5.0×10^{-6} and 1.4×10^{-6} M, respectively. Bethanechol, which induced only 23% of the maximal effect obtained by acetylcholine, was a partial agonist with an ED_{50} of 4.8×10^{-4} M. Its antagonistic component is expressed by an inhibition constant of 1.9×10^{-4} M. In parallel, binding studies were performed in a competition assay with [^{3}H]-quinuclidinylbenzilate. For the agonists acetylcholine and carbachol, binding parameters were best fitted by a "two binding-sites model." Comparison with dose-response curves indicated that Ca^{2+} mobilization was triggered via the high-affinity binding site. The inhibition constants of antagonists derived from the shift of dose-response curves corresponded to the fitted K_D values of the binding studies when a "one binding-site model" was applied. Combination of dose-response and binding data showed close proportionality between receptor occupancy and calcium mobilization. No spare receptors were present.

Undifferentiated cells of the chick limb bud possess a muscarinic cholinergic receptor (1) which is assumed to be part of an embryonic cholinergic system that is expressed in undifferentiated cells during distinct phases of morphogenesis (2, 3). In a preceding publication, we described intracellular Ca^{2+} mobilization upon stimulation of the receptor (4). Ca^{2+} mobilization was measured in a spectrofluorometric assay with chlorotetracycline (CTC)[1] (5, 6). On addition of muscarinic agonists, the cells responded with a fluorescence decrease. The reaction was blocked by muscarinic antagonists. Nicotinic drugs were ineffective.

For further characterization of the muscarinic receptor on embryonic cells, dose-response curves have to be established. Intracellular Ca^{2+} mobilization is a biological effect that can be used for this purpose. In the present study, to quantify CTC fluorescence changes, we standardized the fluorometric measurements and improved data processing. The dose-response curves have to be related to receptor occupancy. Since ligand affinities in homogenate are different from those in cell suspensions, our binding data from homogenate (1) cannot be used for discussion of dose-response curves. In particular, binding of muscarinic agonists in homogenate is influenced by incubation conditions (7) and concentration of metabolites such as guanosine triphosphate (8). Therefore, in the present study, we determined binding of muscarinic ligands in cell suspensions in parallel to the fluorometric measurements. A binding assay with [^{3}H]-quinuclidinylbenzilate (QNB) was established. Instead of the filter assay used for homogenate, we separated bound and free radioactivity by centrifugation. In contrast to the previous study in which cell suspensions from chick limb buds of stage 23/24 were used, we isolated

[1] *Abbreviations used in this paper:* B_{max}, total concentration of specific binding sites; CTC, chlorotetracycline; cv, coefficient of variation; ED_{50}, the agonist concentration that yields 50% of maximal effect; MSE, mean square error; QNB, quinuclidinylbenzilate.

the cells from whole embryos stage 23/24 in order to obtain the large numbers of cells necessary for serial measurements.

MATERIALS AND METHODS

Drugs and Chemicals: Enzymes and Dulbecco's modified Eagle's medium ($NaHCO_3$ omitted, 20 mM HEPES supplemented) were provided by Boehringer GmbH (Mannheim, Federal Republic of Germany [FRG]). The other chemicals were purchased from the following sources: tritium-labeled (32 Ci/mmol) and unlabeled QNB (Radiochemical Centre, Amersham, U.K.), atropine sulfate (Merck AG, Darmstadt, FRG), pirenzepine dihydrochloride (Thomae, Biberach, FRG), acetylcholine chloride, bethanechol chloride, oxotremorine, carbachol chloride (carbamylcholine chloride), pilocarpine hydrochloride, chlorotetracycline hydrochloride, and physostigmine sulfate (Sigma Chemie GmbH, München, FRG). Dexetimide and levetimide are gifts from Janssen GmbH (Neuss-Rosellen, FRG).

Fluorometric Measurements: Cell suspensions of whole chick embryos stage 23/24 were prepared by enzymatic digestion according to the procedure outlined in a previous publication (4). Cells were stored up to 5 h in tissue culture medium (Dulbecco's modified Eagle's medium). Before loading the cells with CTC, we transferred them into Hanks' solution (1.26 mM Ca^{2+}) without $NaHCO_3$ that contained 20 mM HEPES, pH 7.3, at 37°C. For dose-response curves, up to five matched probes were prepared from a single batch of cells. The cell suspensions were prestained with CTC (20 μM) in a roller culture apparatus (six turns per minute) at 37°C for 20 min. Fluorometric measurements were performed in a Yobin Yvon spectrofluorometer JY 3 D as described previously (4). In experiments using acetylcholine for stimulation, physostigmine (1 μM) was added before stimulation.

Binding Assay: Ligand binding in cell suspension was measured by a centrifugation assay using [^{3}H]QNB as the specific ligand for muscarinic binding sites. Two incubations with a total volume of 1,100 μl each were prepared, the first (incubation 1) containing [^{3}H]QNB (0.4 nM) alone, the second (incubation 2) containing [^{3}H]QNB (0.4 nM) and radioinert atropine in excess (1 μm). Reagents and cell suspensions were prepared in Hanks' solution without $NaHCO_3$ containing 20 mM HEPES, pH 7.3, at 37°C. Cell concentration varied between 5×10^6 and 9×10^6 cells/ml (molar concentrations of specific binding sites [B_{max}] between 30 and 60 pM). Incubation was performed in Eppendorf microvials in a shaking water bath (37°C, 75 cycles per minute). After an incubation period of 1.5 h, free and bound radioactivity were separated by centrifugation for 1 min at 7,000 *g* in an "Eppendorf centrifuge 5414." Kinetic experiments revealed that 1.5 h are sufficient to reach equilibrium. The supernatant was pipetted carefully into a scintillation vial containing 15 ml of scintillation fluid (UNISOLVE 1, Zinsser, Frankfurt, FRG). Residuals of supernatant were removed by superficial washing with 200 μl Hanks' solution (0°C) and added to the scintillation vial. Preliminary experiments showed that at 0°C no measurable dissociation of bound [^{3}H]QNB occurred during the washing procedure. The sediment was resuspended in 200 μl Hanks' solution and transferred to a second scintillation vial with 10 ml of scintillator. Incubation cups were washed twice with 200 μl Hanks' solution, the washing being added to the scintillation vial. Radioactivity was counted in a Beckman beta-counter (LS 9800) (Beckman Instruments, Inc., Palo Alto, CA). Counting efficiencies were estimated by external standard (40–43% for supernatants and 42–45% for sediments).

DATA ANALYSIS

Standardization of CTC Fluorescence Changes

Cells were stimulated by adding the drug in a small volume ($\Delta V = 10$ μl) of stem solution to the CTC-stained cell suspension ($V_T = 2$ ml). The decline (ΔI_T) of total fluorescence intensity (I_T) was due to the pharmacological effect of the drug (ΔI_{biol}) and a dilution effect (ΔI_{vol}). The constant α was measured ($\alpha = 0.7$).

$$\Delta I_{vol}/I_T = -\alpha \cdot \Delta V/V_T. \quad (1)$$

$$\Delta I_{biol} = \Delta I_T + \alpha \cdot I_T \cdot \Delta V/V_T. \quad (2)$$

For standardization, ΔI_{biol} is expressed in percentage of the fluorescence of CTC-stained cells (I_{cell}). I_{cell} is the difference between the total fluorescence of the CTC-stained cell suspension (I_T) before stimulation and background fluorescence of the CTC-containing medium without cells (I_{bg}). I_{bg} was determined after removal of cells by centrifugation.

$$I_{cell} = I_T - I_{bg}. \quad (3)$$

$$\Delta I_{stand} = \Delta I_{biol}/I_{cell}. \quad (4)$$

Calculation of Specific Binding

Separation of cell-bound and free radioactivity was performed by rapid centrifugation. Since during centrifugation cells are in continuous contact with the supernatant, the equilibrium between bound and free ligands was maintained during separation. Thus the measured values reflect the true equilibrium concentrations of free and bound radiolabeled ligand in the incubations: Free radioactivities were measured in the supernatants of incubation 1 (F_1) and incubation 2 (F_2), and bound radioactivities were measured in the respective sediments (B_1 and B_2). Usually specific binding is estimated by the difference of bound radioactivity in both incubations:

$$D = B_1 - B_2. \quad (5)$$

In the present study we calculated specific binding as follows:

$$D_{corr} = B_1 - B_2 \cdot F_1/F_2 \quad (6)$$

This formula corrects for systematic underestimation of specific binding by Eq. 5: in incubation 2, total radioactivity contributes to free and nonspecifically bound radioactivity whereas in incubation 1 a fraction of the radioactivity is specifically bound. In the standard incubations ($5–9 \times 10^6$ cells/ml), 20–50 pM of total [^{3}H]QNB (400 pM) was bound specifically and 20–40 pM was bound nonspecifically. Therefore, $F_1 < F_2$ and the values of the correction term F_1/F_2 range between 0.86 and 0.95.

Parameter Fitting

For parameter fitting we used the nonlinear least squares regression program BMDPAR (BMDP statistical software, University of California, 1981) on a UNIVAC 1100/80 computer (Rechenzentrum der Universität Tübingen). Confidence limits were computed as "asymptotic standard deviations" (BMDP manual, 1981). Concentrations were internally transformed to logarithms prior to fitting. Therefore, confidence limits of parameters with the dimension "concentration" (e.g., dissociation constants) sometimes appear unsymmetrical. The goodness of fit of different models to the same data can be compared by the mean square error (MSE) of the fits. The MSE of a fit is equal to the minimal residual sum of squares divided by $(n - p)$, where n is the number of cases and p is the number of independent parameters. Most of the figures, including the fitted curves, were plotted with the DISSPLA software system (Integrated Software Systems Cooperation, San Diego, CA) on a Calcomp plotter connected to the UNIVAC 1100/80.

Dose-Response Curves

Parameters were fitted by assuming one class of noninteracting receptors and proportionality between occupancy and effect (9).

$$\Delta I_{stand} = \Delta I_{max} \cdot [A]/(ED_{50} + [A]), \quad (7)$$

where ΔI_{stand}, the standardized fluorescence decrease (Eq. 4), is the dependent variable and the agonist concentration [A] is the independent variable. The parameter ΔI_{max} signifies the maximal effect and ED_{50} is the agonist concentration yielding 50% of maximal effect.

Addition of a reversible competitive antagonist (I) before stimulation resulted in a shift of the dose-response curve to the right (see Fig. 3). From ED_{50} values of shifted (ED_{50}') and unshifted (ED_{50}) curves, the K_I value of the antagonistic substance can be calculated. Under the assumptions of Clark's model (9), K_I is identical to the dissociation constant of the antagonist (10):

$$K_I = [I] \cdot ED_{50}/(ED_{50}' - ED_{50}). \quad (8)$$

Saturation Studies

Specific binding of [^{3}H]QNB was nonlinearily fitted to the saturation function (9) of a "one-site model" with the parameters B_{max} (total concentration of specific binding sites) and K_D (dissociation constant):

$$[R\text{-}^3HQ] = B_{max} \cdot [^3HQ]/(K_D + [^3HQ]). \quad (9)$$

[^{3}HQ], the equilibrium concentration of free [^{3}H]QNB, is measured as F_1 in the supernatant of incubation 1, and [R-^{3}HQ], the equilibrium concentration of specifically bound [^{3}H]QNB, is calculated as D_{corr} according to Eq. 6.

Competition Curves

The data input of one competition experiment consisted of 12 triplets of values: [A], [^{3}HQ], and [R-^{3}HQ]. The concentration of competitor A was known and [^{3}HQ] and [R-^{3}HQ] were measured as F_1 and D_{corr}. We avoided systematic and random errors due to various concentrations of total and free [^{3}H]QNB in the individual incubations by measuring the concentration of free [^{3}H]QNB individually in each incubation. Competition data were fitted to three models: The first model assumes the competition of [^{3}H]QNB and an unlabeled ligand (A) for a single population of noninteracting binding sites (one-site model):

$$[R\text{-}^3HQ] = \frac{B_{max} \cdot [^3HQ]}{K_Q + [^3HQ] + [A] \cdot K_Q/K_A}. \quad (10)$$

K_Q (the dissociation constant of [^{3}H]QNB derived from saturation studies) has a fixed value ($K_Q = K_D = 10^{-10}$ M; see Table III). [A] is the concentration of competitor and K_A is its dissociation constant. The fitting procedure creates values for the free parameters B_{max} and K_A.

The second model describes the displacement of [^{3}H]QNB by unlabeled ligand which has different affinities for two noninteracting sites (two-sites model):

$$[R\text{-}^3HQ] = \frac{R_H \cdot [^3HQ]}{K_Q + [^3HQ] + [A] \cdot K_Q/K_H} + \frac{R_L \cdot [^3HQ]}{K_Q + [^3HQ] + [A] \cdot K_Q/K_L}. \quad (11)$$

Parameter estimates were created for the concentrations of binding sites showing high affinity (R_H) and low affinity (R_L) towards the competitor and for the respective dissociation constants K_H and K_L.

The third model is derived from the equation of Hill (11) and, in contrast to the models mentioned above, is not a molecular model when the Hill coefficient n_H is not an integer. It gives a phenomenological description of the [^{3}H]QNB binding if the competitor binding demonstrates cooperativity (phenomenological cooperativity model):

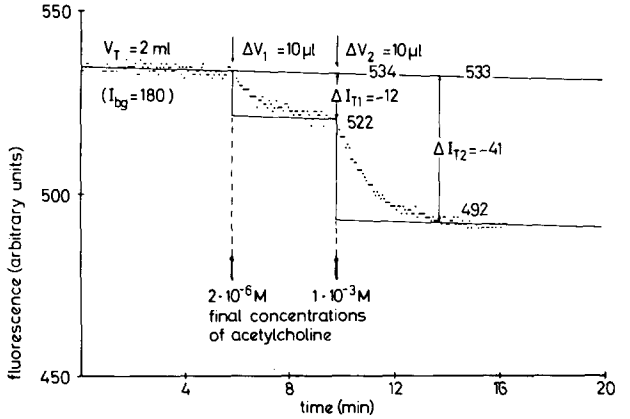

FIGURE 1 Fluorescence decrease in a cell suspension loaded with CTC after stepwise stimulation by acetylcholine. Two consecutive stimulations adding up to the maximal inducible effect are shown. Total fluorescence changes (ΔI_{T1}, ΔI_{T2}) were measured graphically as the difference between total fluorescence (I_T) and fluorescence after stabilization (I_1). On-line plot of fluorescence intensity.

$$[R\text{-}^3HQ] = \frac{B_{max} \cdot [^3HQ]}{K_Q + [^3HQ] + [A]^{nH} \cdot K_Q/K'}. \quad (12)$$

(K' is a constant without physiological meaning.)

RESULTS

Tracing of Ca^{2+} Mobilization by CTC Fluorescence

Cell suspensions loaded with CTC responded to the addition of muscarinic cholinergic agonists with a fluorescence decrease. This decrease indicates receptor-mediated Ca^{2+} mobilization and was documented by continuous tracing in a spectrofluorometer (Fig. 1). The fluorescence intensity is given in arbitrary units which depend on the actual setting of the spectrofluorometer. After addition of a submaximal dose of acetylcholine, total fluorescence (I_{T1}) decreased within 4 min and stabilized on a new plateau (I_1). I_{T1} and I_1 were determined graphically. The fluorescence decrease was obtained by subtraction ($\Delta I_{T1} = I_1 - I_{T1}$). A second stimulation with a higher dose resulted in a further decline of fluorescence intensity (ΔI_{T2} in Fig. 1). After correction of the dilution effect, the drug-induced component of the total fluorescence changes (ΔI_{biol}) was standardized according to Eq. 4. The maximal drug-induced fluorescence decrease was ~15% of cellular fluorescence.

Reproducibility

The standardized fluorescence changes ΔI_{stand} (Eq. 4) measured in different matched probes of one cell preparation (intra-assay variability) showed a variability of cv = 7% (n = 5; cv: coefficient of variation). The ΔI_{stand} values obtained in different preparations of comparable cell suspension (inter-assay variability) revealed a variability of cv = 12% (n = 49). The respective variabilities of the ΔI_{biol} values (Eq. 2) that were not standardized amounted to cv = 12% (intra-assay variability) and cv = 38% (inter-assay variability).

Establishment of Dose-Response Curves

In the experiment of Fig. 1, a first addition of a relatively low concentration of acetylcholine resulted in a submaximal

response. A second stimulation with a higher dose of acetylcholine triggered an additional effect. After the maximal response had been reached, no further reaction was obtained. The dose-response curves described below were established by evaluation of such stepwise stimulation. Three to four additive stimulations could be measured in one probe because the plateau phase lasted only for ~20 min. If more gradations were necessary for a dose-response curve, matched cell suspensions were used.

Reversibility of Reaction

The fluorescence decrease triggered by muscarinic agonists was found to be reversed by the addition of an antagonistic drug. In the experiment shown in Fig. 2, after addition of acetylcholine, the fluorescence was reversed by pilocarpine. As described before (4), in cell suspensions from chick limb bud and from whole chick embryos, pilocarpine antagonizes the acetylcholine-induced Ca^{2+} movement. Reaction and reversal can be repeated several times with increasing concentration of agonists and antagonists. In this respect, pilocarpine and atropine show the same antagonistic behavior. After repetitive stimulation and reversal, the sum of the responses to agonists surmounted the maximal response obtainable without antagonistic reversal. The experiment demonstrated reversibility of ligand binding and repeatability of the drug effects.

In contrast to the fluorescence decrease which lasted 4 min, reversal of the fluorescence decrease by antagonistic substances took ~8 min. In the experiment shown in Fig. 2, pilocarpine was used as the antagonistic substance because its dissociation from the receptor is fast enough to allow further stimulation. For the third reversal (Fig. 2), atropine had to be used, since it is technically impossible to obtain the necessary excess of pilocarpine.

Dose-Response Curves

Fig. 3 shows dose-response curves of the agonists acetylcholine and carbachol and of the partial agonist bethanechol. The standardized effect ΔI_{stand} is depicted against the agonist concentration. The effects were measured as indicated in Fig. 1 and standardized according to Eq. 4.

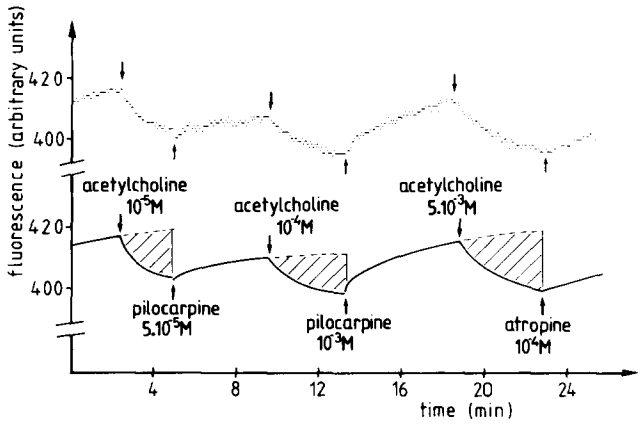

FIGURE 2 Repetitive stimulation and reversion of fluorescence change. After acetylcholine stimulation the effect was antagonized by a relative excess of pilocarpine. The reaction cycle consisting of agonistic stimulation and antagonistic reversal of reaction was triggered a second time with higher concentrations of acetylcholine and pilocarpine. The cycle was repeated a third time with a maximal dose of acetylcholine and reversal by the antagonist atropine.

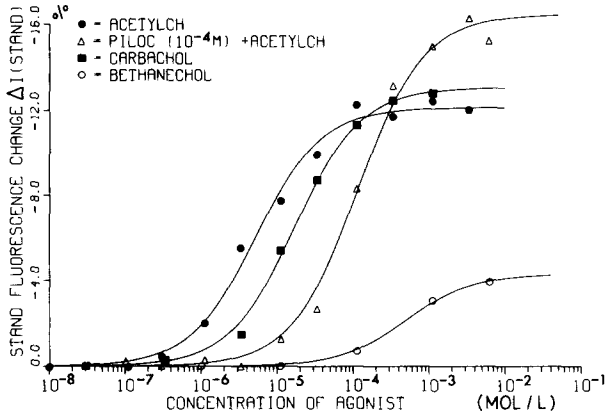

FIGURE 3 Dose-response curves for acetylcholine (*acetylch*) carbachol, and bethanechol fitted according to Eq. 7. Bethanechol triggered only one-third of the maximal inducible response. Previous addition of the reversible competitive antagonist pilocarpine (*piloc*) shifted the dose-response curve of acetylcholine to the right. *STAND*, standard. L, liter.

TABLE I

Parameters of Dose-Response Curves

Substance	ED_{50} (Confidence limits)	*n*	Effect relative to acetylcholine*	*n*
	(*mol/liter*)			
Acetylcholine	3.4×10^{-6} ($2.7\text{–}4.3 \times 10^{-6}$)‡	9	100% by definition	
Carbachol	2.7×10^{-5} ($1.8\text{–}3.9 \times 10^{-5}$)‡	5	92 ± 26%	5
Bethanechol	4.8×10^{-4}§	1	23 ± 9%	5
Oxotremorine	No reaction			
pilocarpine				

Parameters are fitted according to Eq. 7 assuming the simple law of mass action between receptor-mediated effect and agonist concentration using the BMDP software (see Data Analysis). The results are expressed as mean ± SD of several dose-response experiments.

* Expressed as percentage of acetylcholine effect ± SD.

‡ Confidence limits are unsymmetric because means and standard deviations are calculated from logarithms of ED_{50} values.

§ ED_{50} is fitted from the dose-response curve shown in Fig. 3. Therefore no confidence limits are given.

With acetylcholine and carbachol a full effect was obtained, whereas bethanechol triggered only about one fourth the maximal response obtainable with the full agonists. Table I summarizes the data of several experiments in which dose-response curves were established. The ED_{50} of carbachol was one order of magnitude higher than that of acetylcholine. The partial agonist bethanechol had the highest ED_{50}. As outlined in the previous study, oxotremorine and pilocarpine showed no agonistic effect in this system (4).

Influence of Reversible Competitive Antagonists on Dose-Response Curves

Presence of the antagonistic substance pilocarpine in the assay reduced the sensitivity of acetylcholine: Higher concentrations of agonist had to be used to achieve the same effect and the dose-response curve of acetylcholine was shifted to the right (Fig. 3).

From such measurements we were able to determine the K_I values of the antagonists in question according to Eq. 8. The results for five antagonists are shown in Table II. Because of

the antagonistic component of the partial agonist bethanechol, the K_I of this substance could be determined in the competitive assay for antagonists. The ED_{50} value of bethanechol as agonist and its K_I value as antagonist showed similar values (4.8×10^{-4} M and 1.9×10^{-4} M).

According to Furchgott (10, 12), there are two groups of competitive antagonists: "reversible" and "irreversible." The results described above indicate that atropine, pirenzepine, oxotremorine, pilocarpine, levetimide, and bethanechol behave as reversible competitive antagonists in our system.

Influence of Irreversible Competitive Antagonists

As shown in Fig. 4, preincubation of the cell suspension with increasing concentrations of QNB led to a reduction of the maximum effect inducible by acetylcholine. 1×10^{-10} M QNB reduced the maximal response to 50%. The ED_{50} of acetylcholine within the dose-response curves did not change. Therefore, in this context, the antagonist QNB has to be classified as slowly dissociating and thus a practically irreversible competitive antagonist (10, 12). The antagonist dexetimide showed the same behavior, having no effect on the ED_{50} of agonists but reducing the maximum effect (data not shown).

Binding Studies with [^{3}H]QNB

To correlate the effects of muscarinic drugs on Ca^{2+} mobilization with occupancy of the muscarinic receptor, we performed binding studies in cell suspensions. The cell suspensions of whole chick embryos were identical to those used for CTC fluorescence measurements.

TABLE II

K_I Values of Antagonists

Substance	K_I values		No. of independent determinations
	Mean*	Range	
	mol/liter		
Atropine	0.8×10^{-9}	$0.5\text{-}1.3 \times 10^{-9}$	7
Pirenzepine	1.6×10^{-7}	$1.3\text{-}2.0 \times 10^{-7}$	2
Oxotremorine	1.4×10^{-6}	$1.2\text{-}1.7 \times 10^{-6}$	3
Pilocarpine	5.0×10^{-6}	$3.6\text{-}8.2 \times 10^{-6}$	5
Levetimide	8.8×10^{-6}	$5.4\text{-}15 \times 10^{-6}$	3
Bethanechol	1.9×10^{-4}	$1.1\text{-}5.3 \times 10^{-4}$	4

The K_I value is a measure of the antagonistic potency of the respective reversible competitive antagonist. K_I values were calculated according to Eq. 8, where the ED_{50} is the value of the agonist and the ED'_{50} is the value of the dose-response curve after additions of antagonist are inserted.

* Mean values calculated as means of log K_I.

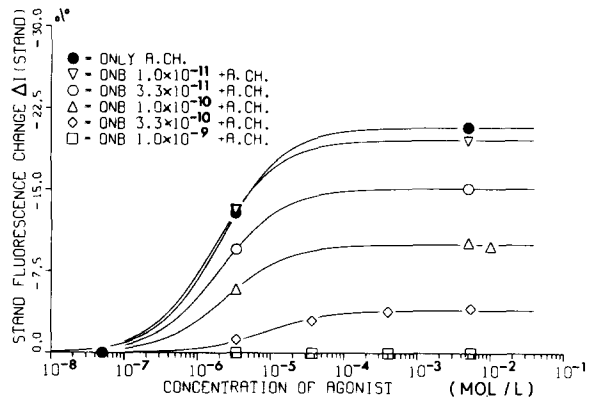

FIGURE 4 Dose-response curve of acetylcholine (*A.CH.*) after equilibration with various concentrations of the antagonist QNB. Increasing QNB concentrations led to a reduction of the maximal inducible effect. *STAND*, standard. L, liter.

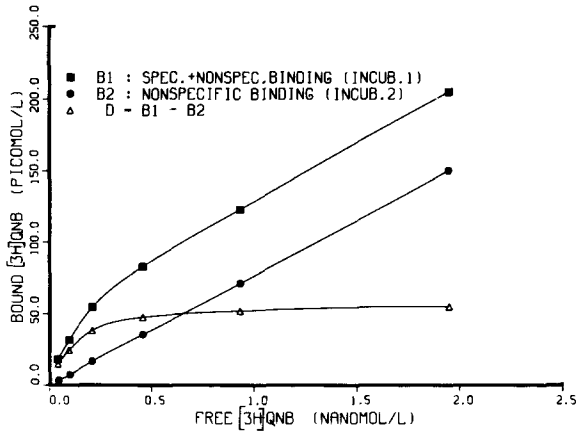

FIGURE 5 Chick embryo cells were incubated with increasing concentrations of the ligand [^{3}H]QNB. In incubation 2 (*incub. 2*) specific binding was suppressed by an excess of radioinert atropine. Nonspecific (*nonspec.*) binding increased proportionally with [^{3}H]QNB concentration. In incubation 1 (*incub. 1*), in addition, specific (*spec.*) binding occurred. Specific binding was calculated from the difference of both curves. L, liter.

The cell suspensions were incubated with the specific muscarinic ligand [^{3}H]QNB for 90 min at 37°C. Separation of cell-bound and free radioactivity was performed by rapid centrifugation. To discriminate specific and nonspecific binding, we performed a second incubation with an excess of unlabeled atropine. Specific binding of [^{3}H]QNB to the cells was calculated according to Eq. 6. The intra-assay variability of the D_{corr} values was determined as cv = 3.4% (n = 12).

Saturation Studies

Fig. 5 shows the determination of specific binding. The curve marked by solid squares gives the total bound radioactivity in incubation 1 with increasing concentrations of [^{3}H]QNB. The curve marked by solid circles gives the linear increase of nonspecific binding as determined in incubation 2. The specifically bound radioactivity (open triangles) shows saturation characteristics.

In Fig. 6, binding data of three saturation experiments are transformed and depicted as Scatchard plots (13). Intersection with the abscissa indicates specific binding capacity B_{max} and the slope indicates the affinity of the specific binding sites for [^{3}H]QNB. All three plots are linear, which indicates a single class of noninteracting specific binding sites. Parameter estimates are given in Table III.

The first saturation experiment of Fig. 6 was performed with a cell suspension from limb buds that at stage 23/24 consists only of undifferentiated cells; the other two experiments used cells of whole chick embryos of the same stage. In the experiment with limb buds, a lower cell concentration was obtained leading to a lower B_{max} value. In addition, the number of binding sites per cell in limb bud was lower than in cell suspensions of whole chick embryos (Table III). The essential feature of the receptor, its affinity, was identical in both preparations.

Competition Studies

In the competition studies the radioinert ligands in question

were added to incubation 1 and 2. From the paired incubations the remaining specific binding of [^{3}H]QNB was calculated. In the resulting competition curves (Fig. 7), three groups of ligands could be distinguished. The first group comprises the antagonists QNB, dexetimide, and atropine. The ID_{50} (concentration of competitor that reduces specific [^{3}H]QNB binding to 50%) values were 10^{-10}, 10^{-9}, and 10^{-8} M, respectively. The second group comprises the antagonistic drugs pirenzepine, oxotremorine, levetimide (not depicted in Fig. 7), and pilocarpine and the partial agonist bethanechol. The respective ID_{50} values ranged between 10^{-6} and 2×10^{-3} M. The third group comprises the fully efficacious agonists acetylcholine and carbachol. The ID_{50} of the agonists ranged between 2×10^{-4} and 2×10^{-3} M. In contrast to the steep competition curves of the antagonists, those of the agonists were flat.

Tables IV + V give the parameter estimates fitted according to the one binding-site model (Eq. 10), the phenomenological cooperativity model (Eq. 12), and the two binding-sites model (Eq. 11) as described in Data Analysis.

For antagonists, the one-site model gave a good fit which was not improved by the phenomenological cooperativity model, as indicated by the MSE (Table IV). For agonists, the fit was considerably improved. Therefore, for agonists the two binding-sites model was applied (Table V).

DISCUSSION

In this paper we describe a muscarinic cholinergic receptor in cell suspensions of the 3½-d chick embryo (stage 23/24). We found that stimulation of the receptor leads to intracellular Ca^{2+} mobilization which is visualized fluorometrically by changes of CTC fluorescence.

In a previous study (1) we have shown that the receptor is present in the undifferentiated limb bud of the same stage. From our histochemical studies we know that in the chick embryo stage 23/24, a large number of undifferentiated cells express embryonic cholinesterase correlated to phases of morphogenesis (2). We therefore assume that the observations in cells of whole embryos reflect reactions of the muscarinic receptor on undifferentiated cells.

Fluorometric Measurements

The decrease of CTC fluorescence intensity after stimulation reflects intracellular Ca^{2+} mobilization (4–6). It is unlikely that in our experiments extracellular Ca^{++} is involved because over a wide range of Ca^{2+} concentrations (0–4 mM) the reaction is independent of the actual extracellular Ca^{2+} level. If the cells are stimulated in Ca^{2+}-free solution in the presence of 0.1 mM EGTA, the reaction remains unchanged, only the repetitivity of the reaction is restricted. If cells are kept in Ca^{2+}-free medium for hours they lose their ability to react presumably owing to depletion of intracellular Ca^{2+} (unpublished results).

In the present experiments the CTC assay was standardized for quantitative evaluation so that dose-response curves and ED_{50} values could be established. The pharmacologic profile of the embryonic muscarinic receptor was found to be as follows: Acetylcholine and carbachol are full agonists whereas bethanechol is a partial agonist (23% of maximal effect). The classical agonists pilocarpine and oxotremorine do not trigger Ca^{2+} mobilization in embryonic cells.

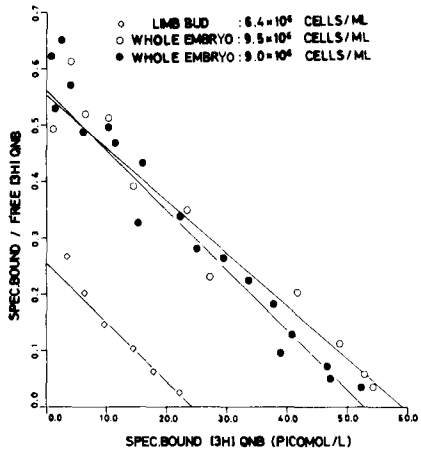

FIGURE 6 Scatchard transformation of three saturation studies results in linear plots. Although the number of binding sites in limb bud cells was less than in cell suspensions of whole embryos, the receptor affinities were the same, as indicated by similar slopes. *Spec.*, specifically. L, liter.

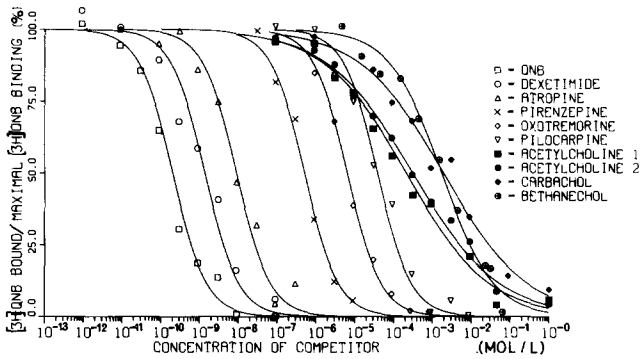

FIGURE 7 In the competition studies with [^{3}H]QNB, the respective muscarinic ligand was added to the incubations in increasing concentrations. Maximal binding was determined without competitor and nonspecific binding in presence of 1 μM atropine. Only the values in the respective saturation range are shown. Curves are fitted as outlined in *Data Analysis*. Parameters are given in Tables IV and V. L, liter.

TABLE III

Binding Parameters of Specific [^{3}H]QNB Binding Sites

Material	Cell concentration	No. of data pairs	K_D	B_{max}	Binding sites per cell
	cells/ml		*10^{-12} mol/liter*		
Chick limb bud	6.4×10^6	6	95 ± 7*	24.2 ± 0.5*	2,300
Whole embryo	9.5×10^6	13	107 ± 8*	59.2 ± 1.4*	3,700
Whole embryo	9.0×10^6	19	94 ± 6*	52.8 ± 1.0*	3,500

Parameters were fitted according to Eq. 9 (see Data Analysis) with the BMDP software (BMDP Statistical Software, University of California, 1981) on the UNIVAC 1100/80 (Rechenzentrum der Universität Tübingen).

* Asymptotic standard deviation (compare BMDP manual, 1981).

TABLE IV

Parameters According to the One-site Model and the Phenomenological Cooperativity Model

Substance	One-site model		Phenomenological cooperativity model	
	K_A (Confidence limits)	MSE	$n_H \pm s^*$	MSE
	(mol/liter)			
QNB	2.9×10^{-11} ($2.4\text{–}3.4 \times 10^{-11}$)	0.89	0.98 ± 0.15	1.0
Dexetimide	3.6×10^{-10} ($2.8\text{–}4.7 \times 10^{-10}$)	1.3	0.63 ± 0.08	0.5
Atropine	1.7×10^{-9} ($1.4\text{–}2.1 \times 10^{-9}$)	1.4	0.79 ± 0.12	1.2
Pirenzepine	1.1×10^{-7} ($0.8\text{–}1.5 \times 10^{-7}$)	3.9	1.31 ± 0.39	4.0
Oxotremorine	1.8×10^{-6} ($1.6\text{–}1.9 \times 10^{-6}$)	0.4	0.95 ± 0.08	0.4
Levetimide	5.4×10^{-6} ($4.2\text{–}7.0 \times 10^{-6}$)	1.6	0.76 ± 0.16	1.5
Pilocarpine	8.8×10^{-6} ($7.2\text{–}11.0 \times 10^{-6}$)	2.8	0.68 ± 0.07	1.3
Acetylcholine 1	3.5×10^{-5} ($2.2\text{–}5.4 \times 10^{-5}$)	5.1	0.41 ± 0.05	0.9
Acetylcholine 2	2.7×10^{-5} ($1.7\text{–}4.1 \times 10^{-5}$)	8.3	0.39 ± 0.06	1.7
Carbachol	2.7×10^{-4} ($1.6\text{–}4.3 \times 10^{-4}$)	8.1	0.41 ± 0.07	1.6
Bethanechol	4.6×10^{-4} ($3.5\text{–}6.1 \times 10^{-4}$)	2.0	0.65 ± 0.09	1.1

Cell suspensions ($5\text{–}9 \times 10^6$ cells/ml; B_{max} = 30–60 pM) were incubated with [^{3}H]QNB (0.4 nM) in the presence of competitors at various concentrations as shown in Fig. 7. For acetylcholine, two independent experiments are shown. Dissociation constants were fitted as logarithms. Confidence limits were calculated from the asymptotic standard deviations (s^*) of the logarithms and, therefore, unsymmetric intervals are given. Parameter values of the one-site model (Eq. 10) and the phenomenological cooperativity model (Hill) (Eq. 12) were fitted, as outlined in Data Analysis, to the data of competition experiments shown in Fig. 7. For antagonistic substances, the one-site model gave a good fit which was not improved by the phenomenological cooperativity model. For the agonists acetylcholine and carbachol, the goodness of fit was clearly improved, as indicated by distinctly reduced MSE. K_A, dissociation constant of the one-site model; n_H, Hill coefficient.

TABLE V

Parameters According to the Two-sites Model

Substance	$R_H \pm s^*$ (%B_{max})	K_H (Confidence limits)	$R_L \pm s^*$ (%B_{max})	K_L (Confidence limits)	MSE
	pmol/liter	*mol/liter*	*pmol/liter*	*mol/liter*	
Acetylcholine 1	15.3 ± 1.6 (53)	3.9×10^{-6} ($2.6\text{–}5.9 \times 10^{-6}$)	13.8 ± 1.7 (47)	0.95×10^{-3} ($0.5\text{–}1.7 \times 10^{-3}$)	1.1
Acetylcholine 2	20.9 ± 1.9 (52)	4.4×10^{-6} ($3.1\text{–}6.3 \times 10^{-6}$)	19.4 ± 2.5 (48)	1.3×10^{-3} ($0.7\text{–}2.1 \times 10^{-3}$)	1.6
Carbachol	14.6 ± 2.0 (44)	1.7×10^{-5} ($1.1\text{–}2.6 \times 10^{-5}$)	18.4 ± 2.0 (56)	2.6×10^{-3} ($1.6\text{–}4.1 \times 10^{-3}$)	1.1
Bethanechol	9.1 ± 3.2 (31)	2.6×10^{-5} ($1.0\text{–}6.9 \times 10^{-5}$)	19.9 ± 3.1 (69)	1.3×10^{-3} ($0.8\text{–}2.0 \times 10^{-3}$)	0.9

Cell suspensions ($5\text{–}9 \times 10^6$ cells/ml; B_{max} = 30–60 pM) were incubated with [^{3}H]QNB (0.4 nM) in the presence of competitors at various concentrations as shown in Fig. 7. For acetylcholine, two independent experiments are shown. Dissociation constants were fitted as logarithms. Confidence limits were calculated from the asymptotic standard deviations (s^*) of the logarithms, and thus unsymmetric intervals are given. Parameter values of the two-sites model (Eq. 11) were fitted for the agonists. The two-sites model gave a better explanation for binding of agonists. R_H and K_H, receptor capacity and dissociation constant of high affinity binding sites; R_L and K_L, receptor capacity and dissociation constant of low-affinity binding sites; R_H and R_L are given in percentage of total binding capacity (% B_{max}).

When antagonists were added before stimulation by an agonist, two distinct patterns were observed. The first class of antagonists shifted the dose-response curve into higher concentration ranges without lowering the maximal effect and without affecting the shape of the curve (Fig. 3). According to Furchgott (10, 12), these compounds are classified as reversible competitive antagonists. The classical muscarinic antagonists atropine, pirenzepine, and levetimide belong to this group as well as the classical muscarinic agonists oxotremorine and pilocarpine. The partial agonist bethanechol also shifts the dose-response curve of a full agonist to the right. From the shift of dose-response curves, we determined the inhibitory constants (K_I values; Table II).

The second class of antagonists, comprising QNB and dexetimide, led to dose-dependent diminution of maximal effect, the ED_{50} remaining nearly unchanged (Fig. 4). According to Furchgott (10, 12) these compounds are classified as irreversible competitive antagonists. The term "irreversible" in this context states that the compounds of this group dissociate so slowly from the receptor sites that during the time course in which the biological effect is observed (20 min), the blockade seems to be irreversible. In our system, the half-life

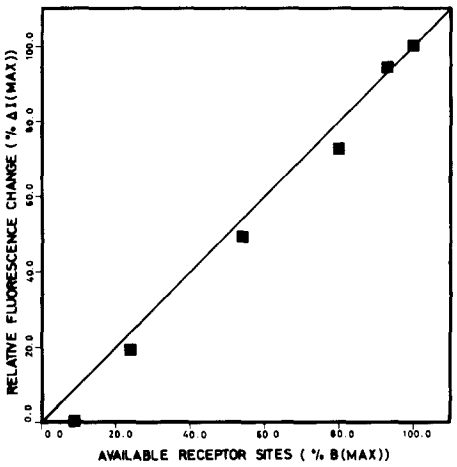

FIGURE 8 The fraction of unblocked binding sites at a given QNB concentration (abscissa) is correlated with the maximal effect obtained by saturating agonist concentrations at the same QNB concentration (ordinate). The fluorescence changes were obtained from the dose-response curves after preincubation with various concentrations of QNB (Fig. 4). The fraction of receptor sites available at the respective QNB concentration was calculated from the dissociation constant derived from the saturation studies (Fig. 6 and Table III).

of the QNB–receptor complex (at 37°C) is 4–5 h (unpublished data).

When added after stimulation, all antagonistic compounds including oxotremorine and pilocarpine were capable of reversing the agonist-induced Ca^{2+} mobilization. Fig. 2 illustrates that stimulation by agonist and reversal by a reversible competitive antagonist could be repeated several times in the same cell suspension. The reversibility and repeatability of the effects are strong arguments for the biological character of the reaction.

Binding Studies

In parallel to the fluorometric measurements, we determined the muscarinic binding sites using [^{3}H]QNB as the ligand. Separation of bound and unbound radioactivity by centrifugation maintained the equilibrium and thus yielded unbiased values as compared with a filter assay. By measuring unbound [^{3}H]QNB in every incubation, we were able to correct for errors due to differing amounts of unbound [^{3}H]QNB in the individual incubations. This avoids systematic errors in the calculation of specific binding (Eq. 6) and in the parameter fits.

The Scatchard plots indicate the existence of a single population of noninteracting specific binding sites for [^{3}H]QNB (Fig. 6 and Table III). In the competition studies the antagonists showed steep sigmoid curves whereas for the agonists acetylcholine and carbachol flat competition curves were obtained (Fig. 7). The binding data of antagonistic compounds are in agreement with the assumption of a single class of binding sites (one-site model, Table IV). The observation of a single class of noncooperating binding sites for muscarinic antagonists is in accordance with results of Birdsall and Hulme (14, 15). For the agonists acetylcholine and carbachol, the phenomenological cooperativity model resulted in a distinctly better fit than the one-site model (Table IV). The Hill coefficients between 0.38 and 0.41 indicate negative cooperativity of agonist binding. This is a general finding in agonist binding of muscarinic receptors which is usually explained by assuming at least two distinct classes of noninteracting binding sites with different affinities for agonists (16, 17). Table V gives the fitted parameter values if a two-sites model is assumed. Our data don't allow for the extraction of a third class of "super high-affinity sites" as described in rat brain (16, 18). The binding data of the partial agonist bethanechol are explained by both agonistic and antagonistic behavior (Fig. 7 and Tables IV and V).

Correlation of Ca^{2+} Mobilization and Receptor Occupancy

The K_I values of antagonists determined from the shift of dose-response curves (Table II) are in good agreement with the K_D values calculated according to the one-site model (K_A values Table IV). In the fluorometric measurement, oxotremorine and pilocarpine were observed to behave as antagonists. In the binding studies they showed competition curves with one K_D and no signs of cooperativity. This binding behavior is characteristic of antagonists.

From the dose-response curves the ED_{50} of acetylcholine were quantitated as $3.4 \times {}^{-6}$ M (Table I). This value is nearly equal to the K_D of the high-affinity site (K_H in Table V) of the two-sites model. The same holds true for the ED_{50} and the K_H value of the high-affinity binding site of carbachol. We conclude that in chick embryo cells, the biological effect of Ca^{2+} mobilization is triggered via the high-affinity binding site. Accordingly, the agonistic component of the partial agonist bethanechol was expressed in the high-affinity binding site when competition data were fitted for the two-sites model (Table V). Declining pharmacological activities (Table I) correlated with declining affinities of high-affinity binding sites (K_H in Table V) and with declining ratios of high- to low-affinity binding sites (R_H/R_L in Table V). The dissociation constant of the low-affinity binding sites (K_L in Table V) remained nearly constant. Thus, biological activity seems to be independent of low-affinity binding sites. Correlation between high-affinity muscarinic binding sites and Ca^{2+} influx into smooth muscle cells was described by Triggle (19). Other authors, however, relate biological responses to low-affinity muscarinic binding sites (17, 20–23).

Fig. 8 correlates the maximal Ca^{2+} mobilization that can be induced in embryonic cells by muscarinic agonists with the fraction of muscarinic receptor sites occupied by an agonist. The number of available receptor sites is varied by preincubation with the irreversible competitive antagonist QNB as shown in Fig. 4. 100% of the relative fluorescence change was obtained without QNB. Gradual blocking of binding sites by QNB led to a proportional diminution of the biological effect that can be triggered by saturating concentrations of agonists. The inducible Ca^{2+} mobilization was proportional to the number of available binding sites. No spare receptors were present.

The authors wish to thank Mrs. Annamaria Show and Mrs. Andrea Zürn for excellent technical assistance.

This study was supported by Deutsche Forschungsgemeinschaft ("Embryonale Cholinesterase," Dr 94/5-2).

Received for publication 3 May 1984, and in revised form 5 November 1984.

REFERENCES

1. Schmidt, H. 1981. Muscarinic acetylcholine receptor in chick limb bud during morphogenesis. *Histochemistry.* 71:89–98.
2. Drews, U. 1975. Cholinesterase in embryonic development. *Prog. Histochem. Cytochem.* 7:No. 3. 52 pp.
3. Reich, A., and U. Drews. 1983. Choline acetyltransferase in the chick limb bud. *Histochemistry.* 78:383–389.
4. Schmidt, H., G. Oettling, T. Kaufenstein, G. Hartung, and U. Drews. 1984. Intracellular calcium mobilization on stimulation of the muscarinic cholinergic receptor in chick limb bud cells. *Roux's Arch. Dev. Biol.* 194:44–49.
5. Caswell, A. H. 1972. The migration of divalent cations in mitochondria visualized by a fluorescent chelate probe. *J. Membr. Biol.* 7:345–364.
6. Caswell, A. H., and J. D. Hutchinson. 1971. Visualization of membrane bound cations by a fluorescent technique. *Biochem. Biophys. Res. Commun.* 42:43–49.
7. Hedlund, B., and T. Bartfai. 1978. The importance of thiol- and disulfide groups in agonist and antagonist binding of the muscarinic receptor. *Mol. Pharmacol.* 15:531–544.
8. Ehlert, F. J., W. R. Roeske, and H. I. Yamamura. 1983. The nature of muscarinic receptor binding. In Handbook of Psychopharmacology. L. L. Iverson, S. D. Iversen, and S. H. Snyder, editors. Plenum Press, New York 17:242–283.
9. Clark, A. J. 1933. The Mode of Action of Drugs on Cells. E. Arnold (Publishers) Ltd., London. 299 pp.
10. Furchgott, R. F. 1955. The pharmacology of vascular smooth muscle. *Pharmacol. Rev.* 7:183–265.
11. Hill, A. V. 1909. The mode of action of nicotine and curarine determined by the form of the concentration curve and the method of temperature coefficients. *J. Physiol. (Lond.).* 30:361–373.
12. Furchgott, R. F. 1954. Dibenamine blockade in strips of rabbit aorta and its use in differentiating receptors. *J. Pharmacol.* (Paris). 111:265–284.
13. Scatchard, G. 1949. The attractions of proteins for small molecules and ions. *Ann. NY Acad. Sci.* 51:660–672.
14. Birdsall, N. J. M., and E. C. Hulme. 1976. Biochemical studies on muscarinic acetylcholine receptors. *J. Neurochem.* 27:7–16.
15. Hulme, E. C., N. J. M. Birdsall, A. S. V. Burgen, and P. Metha. 1978. The binding of antagonists to brain muscarinic receptors. *Mol. Pharmacol.* 14:737–750.
16. Birdsall, N. J. M., A. S. V. Burgen, and E. C. Hulme. 1978. The binding of agonists to brain muscarinic receptors. *Mol. Pharmacol.* 14:723–736.
17. Fisher, S. K., P. D. Klinger, and B. W. Agranoff. 1983. Muscarinic agonist binding and phospholipid turnover in brain. *J. Biol. Chem.* 258:7358–7363.
18. Birdsall, N. J. M., E. C. Hulme, and A. S. V. Burgen. 1980. The character of the muscarinic receptors in different regions of the rat brain. *Proc. R. Soc. Lond. B Biol. Sci.* 207:1–12.
19. Triggle, D. J. 1979. The muscarinic receptor: structural, ionic, and biochemical implications. *In* Recent Advances in Receptor Chemistry. F. Gualtieri, M. Gianelli, and C. Melchiorre, editors. Elsevier/North-Holland Biomedical Press, New York. 127–146.
20. Hanley, M. R., and L. L. Iversen. 1978. Muscarinic cholinergic receptors in rat corpus striatum and regulation of guanosine cyclic 3,5-monophosphate. *Mol. Pharmacol.* 14:246–255.
21. Strange, P. G., A. J. M. Birdsall, and A. S. V. Burgen. 1977. Occupancy of muscarinic acetylcholine receptors stimulates a guanylcyclase in neuroblastoma cells. *Biochem. Soc. Trans.* 5:189–191.
22. Birdsall, N. J. M., A. S. V. Burgen, and E. C. Hulme. 1977. Correlation between the binding properties and pharmacological responses of muscarinic receptors. *In* Cholinergic Mechanisms and Psychopharmacology. D. J. Jenden, editor. Plenum Press, New York. 25–33.
23. Birdsall, N. J. M., C. P. Berrie, A. S. V. Burgen, and E. C. Hulme. 1980. Modulation of the binding properties of muscarinic receptors: evidence for receptor-effector coupling. *In* Receptors for Neurotransmitters and Peptide Hormones. G. Pepeu, M. J. Kuhar, and S. J. Enna, editors. Raven Press, New York. 107–116.